Received: 24 August 2018 | Revised: 24 October 2018 | Accepted: 27 November 2018

DOI: 10.1111/gbi.12329

Check for updates

ORIGINAL ARTICLE

WILEY gebiology

Absence of biomarker evidence for early eukaryotic life from the Mesoproterozoic Roper Group: Searching across a marine redox gradient in mid-Proterozoic habitability

Kevin Nguyen[1] | Gordon D. Love[1] | J. Alex Zumberge[1] | Amy E. Kelly[2] | Jeremy D. Owens[3] | Megan K. Rohrssen[4] | Steven M. Bates[1] | Chunfang Cai[5] | Timothy W. Lyons[1]

[1]Department of Earth Sciences, University of California, Riverside, California

[2]Shell International Exploration and Production, Houston, Texas

[3]Department of Earth, Ocean & Atmospheric Sciences, Florida State University, Tallahassee, Florida

[4]Department of Earth & Atmospheric Sciences, Central Michigan University, Mount Pleasant, Michigan

[5]Institute of Geology and Geophysics, Chinese Academy of Sciences, Beijing, China

Correspondence
Gordon D. Love and Timothy W. Lyons, Department of Earth Sciences, University of California, Riverside, CA.
Emails: glove@ucr.edu (GDL) and timothyl@ucr.edu (TWL)

Funding information
Directorate for Geosciences; NASA Astrobiology Institute, Grant/Award Number: NNA15BB03A

Abstract

By about 2.0 billion years ago (Ga), there is evidence for a period best known for its extended, apparent geochemical stability expressed famously in the carbonate–carbon isotope data. Despite the first appearance and early innovation among eukaryotic organisms, this period is also known for a rarity of eukaryotic fossils and an absence of organic biomarker fingerprints for those organisms, suggesting low diversity and relatively small populations compared to the Neoproterozoic era. Nevertheless, the search for diagnostic biomarkers has not been performed with guidance from paleoenvironmental redox constrains from inorganic geochemistry that should reveal the facies that were most likely hospitable to these organisms. Siltstones and shales obtained from drill core of the ca. 1.3–1.4 Ga Roper Group from the McArthur Basin of northern Australia provide one of our best windows into the mid-Proterozoic redox landscape. The group is well dated and minimally metamorphosed (of *oil window* maturity), and previous geochemical data suggest a relatively strong connection to the open ocean compared to other mid-Proterozoic records. Here, we present one of the first integrated investigations of Mesoproterozoic biomarker records performed in parallel with established inorganic redox proxy indicators. Results reveal a temporally variable paleoredox structure through the Velkerri Formation as gauged from iron mineral speciation and trace-metal geochemistry, vacillating between oxic and anoxic. Our combined lipid biomarker and inorganic geochemical records indicate at least episodic euxinic conditions sustained predominantly below the photic zone during the deposition of organic-rich shales found in the middle Velkerri Formation. The most striking result is an absence of eukaryotic steranes (4-desmethylsteranes) and only traces of gammacerane in some samples—despite our search across oxic, as well as anoxic, facies that should favor eukaryotic habitability and in low maturity rocks that allow the preservation of biomarker alkanes. The dearth of Mesoproterozoic eukaryotic sterane biomarkers, even within the more oxic facies, is somewhat surprising but suggests that controls such as the long-term nutrient balance and other environmental factors may have throttled the abundances and diversity of early eukaryotic life relative to bacteria within marine

 © 2019 John Wiley & Sons Ltd

microbial communities. Given that molecular clocks predict that sterol synthesis evolved early in eukaryotic history, and (bacterial) fossil steroids have been found previously in 1.64 Ga rocks, then a very low environmental abundance of eukaryotes relative to bacteria is our preferred explanation for the lack of regular steranes and only traces of gammacerane in a few samples. It is also possible that early eukaryotes adapted to Mesoproterozoic marine environments did not make abundant steroid lipids or tetrahymanol in their cell membranes.

1 | INTRODUCTION

The mid-Proterozoic (2.0–1.0 Ga) is well known for its long-lived geochemical stasis, showing only subtle variation in carbonate $\delta^{13}C$ spanning this interval (Brasier & Lindsay, 1998). By the end of this time interval, the major clades of crown eukaryotes had diverged (Parfrey, Lahr, Knoll, & Katz, 2011), but their evolutionary development was apparently stifled so that diversity patterns and abundances were persistently low compared to the later Neoproterozoic (Knoll, Javaux, Hewitt, & Cohen, 2006). Past work has suggested that low-oxygen contents and related limited availability of critical nutrients in the ocean may have contributed to the apparent biogeochemical and paleobiological stasis (Derry, 2015; Laakso & Schrag, 2017; Lyons, Reinhard, & Planavsky, 2014; Reinhard et al., 2013, 2016). Despite important innovations during this interval, this apparent monotony relative to the events that followed has led to the common referral of the period 2.0 and 1.0 Ga as the "dullest time in Earth's history" (Brasier & Lindsay, 1998; Buick, Des Marais, & Knoll, 1995).

Our current understanding of the redox chemistry of the mid-Proterozoic ocean is that the surface waters were most likely oxygenated, while the deeper low-oxygen waters were marked by sulfidic (euxinic) zones at intermediate depths, particularly along the highly productive ocean margins (Canfield, 1998). Iron-rich anoxic (ferruginous) conditions dominated at greater depth (Lyons, Reinhard, & Scott, 2009; Planavsky et al., 2011; Poulton & Canfield, 2011). The redox structure of the ocean at that time may have influenced the patterns and rates of evolution by modulating the spatiotemporal distribution of essential macro- and micronutrients, as well as overall availability of oxygen (Anbar & Knoll, 2002; Derry, 2015; Laakso & Schrag, 2017; Lyons et al., 2014; Reinhard et al., 2013, 2016). It has been suggested that biological feedbacks, including sulfide-based anoxygenic photosynthesis (Johnston, Wolfe-Simon, Pearson, & Knoll, 2009), may have helped maintain a world with low-oxygen levels and sulfide pervasive enough to limit the development and proliferation of early complex life. However, various feedbacks make the persistence of widespread anoxia, particularly euxinia, equally challenging. Specifically, nutrient limitations coupled to widespread anoxia and euxinia (e.g., loss of fixed nitrogen through denitrification and perhaps limited availability of trace-metal micronutrients such as molybdenum) can result in reduced availability of organic matter required to sustain anoxia via aerobic respiration and to support sulfide production via microbial sulfate reduction (Anbar & Knoll, 2002; Scott et al., 2008). The apparent balance among these feedbacks that kept the mid-Proterozoic ocean "dull" remains a topic ripe for further study.

It is widely accepted that the chemistry of the early ocean and life co-evolved. However, the true geochemical nature of Earth's "boring billion" remains poorly constrained. There are many lines of evidence that document an increase in Earth's surface oxidation state approximately 2.4–2.3 Ga (Bekker et al., 2004; Luo et al., 2016), and another biospheric oxygenation estimated between 800 and 550 Ma (reviewed in Och & Shields-Zhou, 2012) that was coincident with a global expansion of eukaryotic abundance in the marine realm (Brocks et al., 2017; Isson et al., 2018). Conditions in the intervening mid-Proterozoic are less studied and correspondingly less known, with the likelihood of intermediate redox states in the ocean and atmosphere. Many of the most-cited data have come from the McArthur Basin of northern Australia. Specifically, shales of the Roper Group in this region have emerged as one of our best archives of mid-Proterozoic ocean redox because the group is well dated, minimally metamorphosed, and lie in the middle of this key interval (Jackson, Sweet, & Powell, 1988). Most importantly, sedimentological and geochemical data suggest a relatively strong connection to the open ocean in mainly an outer shelf setting (Abbott & Sweet, 2000; Jackson, Powell, Summons, & Sweet, 1986; Jackson & Raiswell, 1991; Jackson et al., 1988). As a result, conditions in the Roper Group may reflect the redox state of the global ocean and specifically the conditions that favored, or challenged, the development and expansion of complex life during this interval. Given this potential, we herein report on the first high-resolution, fully integrated geochemical study of the Roper Group—with the goal of performing organic biomarker work within a tight inorganic geochemical context that defines a gradient in habitability and thus potential eukaryotic inhabitation. Our results suggest that controls other than just local redox modulated the distribution of steroid-producing eukaryotes in the mid-Proterozoic ocean.

1.1 | Sampling location

Much of the attention drawn to the McArthur Basin was initially through the discovery of "live oil", originally reported by Jackson et al. (1986). Their findings garnered significant interest in the area, and subsequent investigations have been designed to define its depositional environment. Concisely, the Roper Group within

the McArthur Basin is located at the tip of northern Territory of Australia, near the Gulf of Carpentaria, and occurs over an area of at least 145,000 km^2 with a maximum thickness of approximately 5,000 m (Abbott & Sweet, 2000). The samples in this study are from the Velkerri Formation sampled in the Altree-2 drill core; the Velkerri has a known extent of at least 80,000 km^2 (Jackson & Raiswell, 1991) and is within the oil window, as reflected by its thermal maturity (Crick, 1992; Summons, Taylor, & Boreham, 1994). Jackson, Sweet, Page, and Bradshaw (1999) reported a U-Pb age of 1,492 ± 4 Ma from the lowermost member of the Roper Group, the Mainoru Formation, implying younger ages for the deposition of the Velkerri Formation. Re-Os age constraints yielded age estimates for the base (1,417 ± 29 Ma) and top (1,361 ± 21 Ma) of the Velkerri Formation (Kendall, Creaser, Gordon, & Anbar, 2009), although detrital zircon U-Pb dates suggest that the Velkerri Formation was deposited between 1,349 and 1,320 Ma (Yang et al., 2017). The Altree-2 drill core was sampled over a depth interval of 440–1,250 m, covering the full thickness of the Velkerri Formation. The formation is divided into three informal subunits—the upper (392–672 m), middle (672–948 m), and lower Velkerri (948–1,242 m). The Velkerri Formation strata were likely deposited in a distal marine shelf setting (Abbott & Sweet, 2000). Rock-Eval pyrolysis data (Hydrogen Index, Table 1) independently confirmed that these core samples generally span a thermal maturity range spanning from early oil window to just beyond peak oil window and thus are suitable for detailed organic geochemical investigation since these rocks are thermally well preserved.

2 | METHODS

2.1 | Inorganic geochemistry

Sampling specifically targeted drill core shales to explore the degree of oxygenation within the local water column and to provide added perspective on oxygen in the global ocean. Total carbon (TC), total inorganic carbon (TIC), and total sulfur (TS) were measured by infrared absorption of CO_2/SO_2 using an Eltra CS-500 equipped with a furnace and acidification module. TC and TS were determined via combustion at 1,400°C, while TIC was liberated via reaction with 4 M HCl. Total organic carbon (TOC) was calculated by difference.

Sequential extraction of reactive Fe phases was carried out using the previously described method (Poulton & Canfield, 2005) and analyzed on an Agilent 7500ce quadrupole inductively coupled plasma mass spectrometer (ICP-MS). Reproducibility of Fe speciation measurements, based on replicate analyses within and between sample batches, was better than 93%. Pyrite iron (Fe_{Py}) was quantified using chromous chloride distillation followed by titration with iodine as outlined in Ref. (Canfield, Raiswell, Westrich, Reaves, & Berner, 1986). A pyrite standard was included in every sample batch. Iron relationships were also assessed using the conventional degree of pyritization technique (DOP; Raiswell, Buckley, Berner, & Anderson, 1988), whereby residual (unpyritized) "reactive" Fe is extracted using a boiling, 12 M HCl step. This DOP technique will, if anything, overestimate the truly reactive phases. As such, false positives for euxinia are unlikely, and high DOP values are taken as a particularly robust indicator of that condition in the ancient water column (reviewed Lyons & Severmann, 2006). Once extracted, the amount of iron was quantified spectrophotometrically using the standard ferrozine method. Replicate analysis yielded a standard deviation of 0.25 wt.%.

Pyrite sulfur in the samples was also extracted using the Cr reduction method for sulfur isotope analysis via a silver nitrate trap, rather than the zinc acetate solution used for the pyrite-S quantification by iodometric titration. The resulting silver sulfide was homogenized, weighed with excess V_2O_5, and combusted online for analyses of $^{34}S/^{32}S$ ratios using a Thermo Delta V mass spectrometer, which are reported using the delta notation as per mil (‰) deviations from the Vienna Canyon Diablo Troilite (VCDT) standard. Reproducibility was better than 0.14‰ based on single-run and long-term standard monitoring (additional analytical details for the DOP and $\delta^{34}S$ determinations are provided in the Supporting Information).

A multi-acid digestion technique was employed for trace-metal analysis. Samples were ashed at 900°C for 24 hr, and mass lost through ignition was recorded prior to undergoing acid digestion (HF, HNO_3, and HCl). Analyses were performed on same ICP-MS with the Devonian Ohio Shale (SDO-1) as a reference, with reproducibility in individual runs of better than 95% for the presented elements.

2.2 | Organic geochemistry

2.2.1 | Extraction of free (extractable) biomarker lipids

For organic biomarker analysis, core samples were trimmed with a water-cooled rock saw to remove outer weathered surfaces (typically 5–10 mm thickness was removed) to expose a solid inner portion, which was fragmented. The resulting chips from this inner portion were solvent-rinsed prior to powdering in a zirconia ceramic puck mill within a SPEX 8515 shatterbox. Lipid biomarkers were extracted at 100°C in 9:1 dichloromethane/methanol (v/v) mixture for 15 mins in a CEM Microwave Accelerated Reaction System (MARS). Whole rock bitumens were separated into saturates, aromatics, and polar (N, S, O compounds) fractions by silica column chromatography. Typically 10–20 g of rock powder was used for extraction, yielding from 0.3 to 7.5 mg of bitumen per gram of rock powder (mean = 3.5 mg per gram, Supporting Information Table S5). Full procedural blanks with pre-combusted quartz sand (850°C) were performed in parallel with each batch of rocks to ensure that any background hydrocarbon compounds were negligible in comparison with biomarker abundances.

2.2.2 | Catalytic hydropyrolysis (HyPy) of pre-extracted rocks/kerogens

Pre-extracted rock residues, containing predominantly kerogen, were subjected to continuous-flow catalytic hydropyrolysis (HyPy)

TABLE 1 Selected geochemical data and lipid biomarker ratios for Altree-2 rocks used for organic geochemical investigation

Depth (m)	TOC (wt.%)	HI	S (wt.%)	MPI-1	%Rc	Ts/ (Ts + Tm)	$C_{29}\alpha\beta/C_{30}\alpha\beta$	$C_{30}H$ $\beta\alpha/\alpha\beta$	$C_{31}\alpha\beta S/$ (S + R)	2αMeH (%)	G/H	C_{27} St/ $C_{30}\alpha\beta$	$C_{21} + C_{22}$ St/ $C_{30}\alpha\beta$	Total steranes (ppm sats)	Total hopanes (ppm sats)
452.14–452.22	1.5	–	1.23	0.45	0.67	0.59	0.98	0.06	0.57	5.9	0.04	0.00	0.00	<0.10	2.40
508.35–508.44	1.4	233	0.19	0.59	0.75	0.60	0.80	0.07	0.57	1.7	<0.02	0.00	0.00	<0.10	15.64
561.58–561.64	1.2	279	0.29	0.57	0.74	0.63	0.81	0.07	0.59	2.4	<0.02	0.00	0.00	<0.10	7.00
607.91–607.98	0.4	–	1.13	0.53	0.72	0.43	0.78	0.06	0.56	5.9	<0.02	0.00	0.00	<0.10	2.20
663.83–663.91	5.1	413	1.85	0.51	0.71	0.63	0.78	0.06	0.57	7.1	0.05	0.00	0.00	<0.10	1.80
706.87–706.96	7.8	346	5.10	0.51	0.71	0.62	1.16	0.06	0.55	5.3	<0.02	0.00	0.00	<0.10	6.87
725.76–725.88	7.6	344	3.85	0.49	0.69	0.77	0.65	0.07	0.52	8.2	<0.02	0.00	0.00	<0.10	1.04
852.68–852.76	3.3	267	1.37	0.85	0.91	0.78	0.89	–	0.61	5.3	<0.02	0.00	0.00	<0.10	2.28
932.88–932.92	5.5	216	2.39	0.96	0.98	0.76	0.84	–	0.55	–	<0.02	0.00	0.00	<0.10	0.54
1,124.94–1,124.98	3.6	100	0.66	1.37	1.22	0.71	0.72	–	0.57	–	<0.02	0.00	0.00	<0.10	2.34
1,125.55–1,125.57	3.4	123	0.53	1.41	1.25	–	–	–	–	–	–	–	–	–	–
1,205.18–1,205.20	3.9	53	0.36	1.48	1.29	–	–	–	–	–	–	–	–	–	–

Note. HI: Hydrogen Index (S2*100/TOC) from Rock-Eval (in mg/g TOC); MPI-1: methylphenanthrene index [1.5*(2MP + 3MP)/(1MP + 9MP + P)]; %Rc: vitrinite reflectance equivalence [(0.60*MPI-1) + 0.40]; Ts/(Ts + Tm) for C_{27} hopanes; $C_{29}\alpha\beta/C_{30}\alpha\beta$ for hopanes; $C_{30}\beta\alpha/C_{30}\alpha\beta$ for hopanes; $C_{31}\alpha\beta$ [22S/(22S + 22R)] for hopanes; 2α-methylhopane index = [C_{31} 2αMeH/(C_{31} 2αMeH + C_{30}H) × 100]; G/H: gammacerane/$C_{30}\alpha\beta$ hopane; sterane/hopane ratios from $C_{27}St/C_{30}H$ and ($C_{21}St + C_{22}St$)/$C_{30}H$. Total hopanes (C_{27}–C_{35} abundance in ppm of total saturated hydrocarbons). Total steranes (C_{27}–C_{29} abundance in ppm of total saturated hydrocarbons); –: reliable peak ratios cannot be measured due to low signal for the more mature rocks.

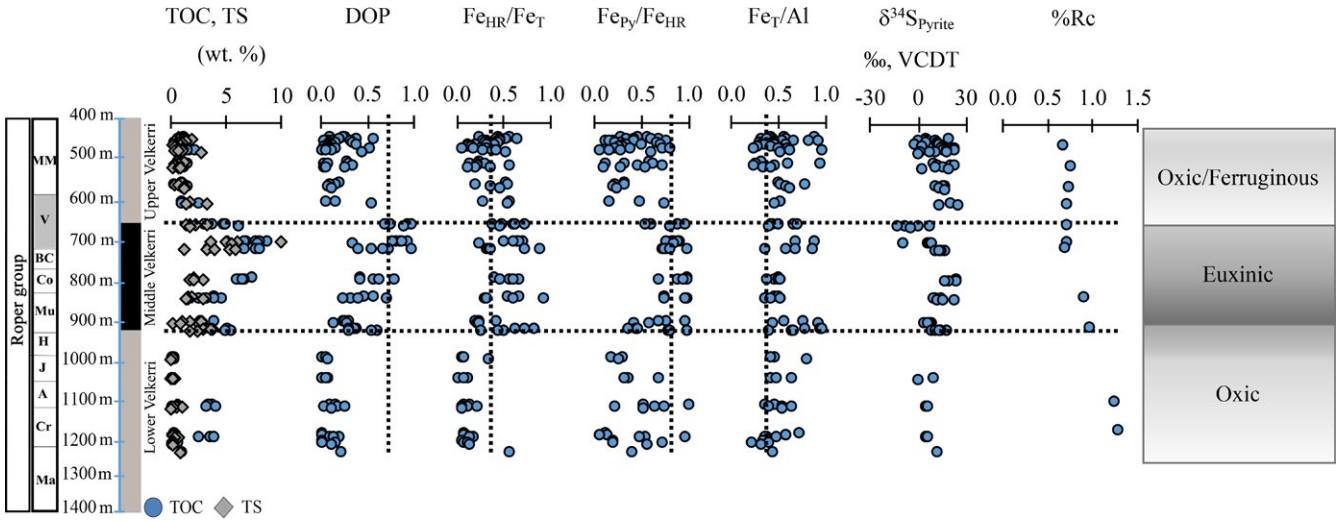

FIGURE 1 Stratigraphic column (emphasizing shales) for drill core Altree-2 for the Velkerri Formation, Roper Group with stratigraphic variations for TOC/TIC/TS, DOP, Fe_{HR}/Fe_T, Fe_{Py}/Fe_{HR}, Fe_T/Al, $\delta^{34}S_{Pyrite}$, and %Rc—showing changes in depositional redox structure. Fe_{HR}/Fe_T ratios >0.4 reflect anoxic deposition. Fe_{Py}/Fe_{HR} ratios above 0.8 reflect euxinic deposition (Poulton & Canfield, 2011). Fe_T/Al ratios below 0.4–0.5 typically reflect oxic settings, while a ratio of 0.6–1.0 likely indicates anoxia/euxinia. Dashed line represents average oxic marine values for the Fe speciation data. %Rc: vitrinite reflectance equivalent; DOP: degree of pyritization; Fe_{HR}: highly reactive iron; Fe_{Py}: pyrite iron; Fe_T: total iron; TIC: total inorganic carbon; TOC: total organic carbon; TS: total sulfur [Colour figure can be viewed at wileyonlinelibrary.com]

to cleave covalent bonds and fragment the kerogen matrix into soluble products (Love, Snape, Carr, & Houghton, 1995; Love et al., 2009) for subsequent GC-MS and MRM-GC-MS analysis. The parallel analyses of covalently bound biomarkers and other bound molecular constituents, alongside the analysis of rock bitumens, give us confidence that we have correctly identified syngenetic compounds and allows us to screen for any significant contamination contributions in an important self-consistency check (Love et al., 2009). Extracted sample powders (~1.0–1.8 g) were secured in the HyPy reactor tube atop a steel wool plug, which was Soxhlet-extracted (DCM, 48 hr) and baked (450°C, 2 hr) to ensure that no contaminates were introduced to the sample. Full procedural HyPy blanks were conducted using clean silica gel as a substrate. Blank HyPy runs were confirmed to be clean and free of contamination, as described in French et al. (2015). HyPy is a temperature programmed pyrolysis method using two temperature ramps: 0–250°C at 100°C/min immediately followed by 250–520°C at 8°C/min while maintaining constant hydrogen pressure of ~15 MPa with a hydrogen sweep gas flow rate of 6 dm^3/min. The pyrolysate was collected in a dry ice-cooled product trap onto silica gel (35–70 mesh, activated at 450°C overnight). After each HyPy run, the silica gel plug from the trap containing the adsorbed pyrolysate product was separated using the same column chromatographic and GC-MS methodology as described for the rock bitumens.

2.2.3 | Lipid biomarker analysis and quantification

Gas chromatography–mass spectrometry (GC-MS) was performed on saturated and aromatic hydrocarbon fractions from rock bitumens and hydropyrolysates in full scan mode over a mass range of 50–600 Da on an Agilent 5975C inert Mass Selective Detector (MSD) mass spectrometer interfaced to an Agilent 7890A GC equipped with a DB-1MS capillary column (60 m × 0.32 mm, 0.25 μm film) and run in splitless injection mode with He as carrier gas. The temperature program for GC-MS full scan was 60°C (2 min), ramped to 150°C at 20°C/min, then to 325°C at 2°C/min, and held at 325°C for 20 min. 200 ng of d_{14}-*p*-terphenyl standard was added to between 1.4 and 12.1 mg of aromatic hydrocarbon fraction as a standard for quantification. MPI-1 index values were calculated using 178 Da peak areas for phenanthrene and 192 Da peak areas for methylphenanthrenes.

To probe polycyclic alkane biomarker distributions in detail, metastable reaction monitoring–gas chromatography–mass spectrometry (MRM-GC-MS) was conducted on the saturated hydrocarbon fractions from rock bitumens and kerogen hydropyrolysates with a Waters AutoSpec Premier mass spectrometer. The spectrometer is equipped with an Agilent 7890A gas chromatograph and DB-1MS coated capillary column (60 m × 0.25 mm, 0.25 μm film thickness) using splitless injection and He for carrier gas. The GC temperature program used for compound separation consisted of an initial hold at 60°C for 2 min, heating to 150°C at 10°C/min, followed by heating to 320°C at 3°C/min, and a final hold at 320°C for 22 min. MRM transitions for C_{27}–C_{35} hopanes, C_{31}–C_{36} methylhopanes, C_{21}–C_{22} and C_{26}–C_{30} steranes, C_{30} methylsteranes, and C_{19}–C_{26} tricyclics were monitored. Biomarker compounds were identified based on retention time and published mass spectra and quantified in MRM-GC-MS by comparison with a deuterated C_{29} sterane internal standard (d_4-ααα-24-ethylcholestane (20R); Chiron Laboratories, AS) assuming equal response factors between sample compounds and the internal standard. Individual yields of hopane and sterane diastereoisomers found in full laboratory procedural blanks were typically <0.1 ng of individual compounds.

3 | RESULTS AND DISCUSSION

3.1 | Total organic carbon, inorganic carbon, and total sulfur

Total organic carbon (TOC) content is appreciable in most of the core samples (Figure 1), with values reaching as high as 8.8 wt.% (Supporting Information Table S1). The lower Velkerri is marked by two episodes where TOC content hovers around 3.5 wt.% on average for a few meters relative to a baseline with near-zero values. The middle Velkerri shows higher TOC contents ranging from roughly 5.5 wt.% at 932 m to a maximum of 8.8 wt.% at 707 m, with a general up-core increase, before oscillating between very low and values as high as 6.2 wt.% in the upper Velkerri. High organic content observed in the Velkerri Formation is interpreted to reflect high but varying organic carbon burial against a backdrop of relatively low clastic dilution (Warren, George, Hamilton, & Tingate, 1998). TIC content for the majority of the samples was consistently low throughout the sequence, ranging from 0 to 1.2 wt.%, with the latter equating to about 10% calcium carbonate. TS behaved similarly to TOC, ranging from values below detection to a maximum of 9.9 wt.% at 707 m in the middle Velkerri before tapering off to low concentrations ranging from values below detection to 1 wt.% in the upper Velkerri (Figure 1 and Supporting Information Table S1).

3.2 | The iron paleoredox proxies and $\delta^{34}S$

Highly reactive iron (Fe_{HR}) is comprised of pyrite iron (Fe_{Py}) and other iron-bearing phases that are reactive toward sulfide in the water column and/or during early diagenesis—that is, ferric (oxyhydr)oxides (Fe_{Ox}), magnetite (Fe_{Mag}), and iron associated with carbonates (Fe_{Carb}; Poulton & Canfield, 2005). Modern marine sediments deposited beneath oxic waters exhibit Fe_{HR}/Fe_T ratios that average about 0.2 and seldom exceed 0.38, which is often treated as the upper limit for oxic deposition (reviewed in Poulton & Canfield, 2011). Values well above this threshold imply anoxic deposition (Raiswell & Canfield, 1998); caution must be exercised when interpreting data that fall near the threshold value. The ratio for total iron to aluminum, Fe_T/Al, can also be used as an indicator for water column anoxia if Fe enrichments are significantly above the average for continental crust (Lyons & Severmann, 2006; Taylor & McLennan, 1985). If anoxia is indicated by high Fe_{HR}/Fe_T and Fe_T/Al ratios, the Fe_{Py}/Fe_{HR} ratio can further distinguish between anoxia and euxinia. Under euxinic conditions, appreciable Fe^{2+} and solid highly reactive Fe phases cannot coexist simultaneously with free H_2S in the water column—with the result of near-complete conversion of Fe_{HR} to pyrite and thus high Fe_{Py}/Fe_{HR} ratios.

Values for Fe_{HR}/Fe_T and Fe_T/Al in the lower Velkerri are consistent with oxic deposition (Figure 1 and Supporting Information Tables), with ratios falling below 0.2 and slightly above 0.4, respectively. However, oxic deposition can be difficult to delineate using the iron proxies because rapid sedimentation can dilute the reactive Fe pool (as well as redox-sensitive trace metals)—that is, the enrichments that are diagnostic of anoxic conditions—via extreme detrital inputs (Lyons & Severmann, 2006). However, Fe_{HR}/Fe_T values in the middle and upper units are often elevated, and the persistence of shales throughout all three subunit makes it difficult to argue for significant temporal changes in rates or patterns of sedimentation as related, for example, to varying water depth. Moreover, previous work has shown that comprehensive dilution of the Fe_{HR} enrichments that are diagnostic of anoxia seems to require extremely high rates of sedimentation (Lyons & Severmann, 2006). Although false positives for oxic deposition are possible, we should be able to recognize these extremes using standard sedimentological and stratigraphic criteria. Finally, the presence of some high values for Fe_{Py}/Fe_{HR} in the lower interval, despite low Fe_{HR}/Fe_T, suggests sulfidic buildup in pore fluids beneath oxic bottom waters, as is observed in marine sediments today (Canfield, Raiswell, & Bottrell, 1992). The higher observed organic contents of these thin intervals, relative to those immediately above and below, would have favored intense diagenetic pyrite formation.

A water column transition to euxinia during deposition of the middle Velkerri is suggested by simultaneously elevated Fe_{HR}/Fe_T, Fe_T/Al, and Fe_{Py}/Fe_{HR}. These values taper off gradually up section at around 850 m and become pronounce again at 725 m, suggesting a transient euxinic phase followed by persistent euxinia. Euxinia is also convincingly indicated for this middle interval by high DOP values that approach 1.0 near the top (Figure 1). The same upper portion of the middle interval is also marked by an obvious decrease in $\delta^{34}S$ values. Such isotopically light values can be interpreted to reflect a predominance of water column (euxinic) pyrite formation under open-system conditions (Lyons, 1997). The remaining values show the ^{34}S enrichments that are typical of the mid-Proterozoic, which are often attributed to generally low sulfate availability in the ocean at this time (Canfield, Farquhar, & Zerkle, 2010; Kah, Lyons, & Frank, 2004; Shen, Knoll, & Walter, 2003). The heaviest value, +25.8‰, occurs in the upper Velkerri and closely matches a past estimate for the isotopic composition of coeval seawater sulfate (Muir, Donnelly, Wilkins, & Armstrong, 1985). Toward the upper Velkerri, values for Fe_T/Al remain elevated, while those of Fe_{HR}/Fe_T oscillate—suggesting ferruginous and oxic conditions. Ferruginous rather than euxinic conditions are confirmed by intermediate Fe_{Py}/Fe_{HR} ratios. Overall, the iron proxies suggest a textured paleoredox structure for Velkerri Formation—from oxic grading toward euxinic in the lower Velkerri, then transiently euxinic to persistently euxinic in the middle Velkerri, and finally oscillating between ferruginous and oxic conditions in the upper Velkerri.

3.3 | Trace-metal proxies

Molybdenum (Mo), uranium (U), and vanadium (V) concentrations (Figure 2 and Tables in Supporting Information) are at crustal levels in the lower Velkerri but reach a maxima of 105 ppm for Mo and 21 ppm for U in the middle Velkerri. Similar values for Mo and U were previously observed from the same units by Kendall et al.

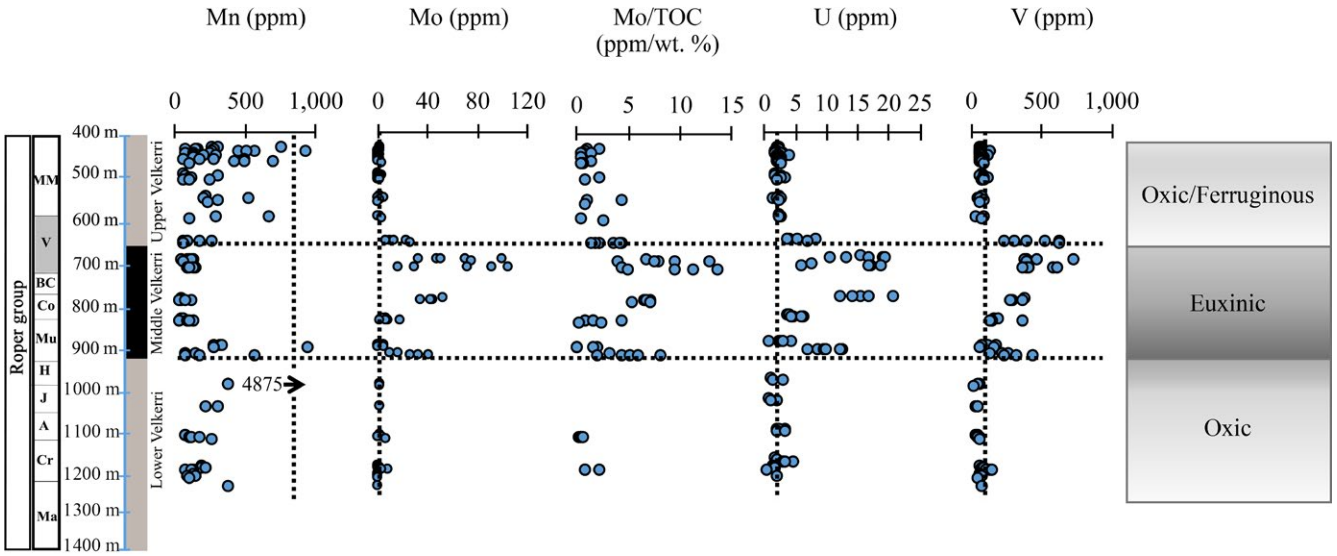

FIGURE 2 Chemostratigraphic records for Altree-2 drill core for the Velkerri Formation, Roper Group with stratigraphic variations of: Mn; Mo; Mo/TOC; U; V; and the prevalent marine redox conditions for each interval. Mo/TOC panel has been culled (TOC with values <1 wt.% were not included) to accurately reflect the covariation. Dashed line in trace-metal panels represents average values of the continental crust. Mn: Manganese; Mo: molybdenum; TOC: total organic carbon; U: uranium; V: vanadium [Colour figure can be viewed at wileyonlinelibrary.com]

(2009) and Partin et al. (2013), respectively. Mo, U, and V concentrations return to crustal levels in the upper Velkerri. Strong enrichment in Mo convincingly argues for euxinic deposition because Mo burial is favored under reducing conditions marked by appreciable H_2S in the water column, with the lower enrichments being characteristic of sulfide that is confined to the pore waters (Scott & Lyons, 2012). Molybdenum enrichment can also track the availability of organic carbon in euxinic systems (Algeo & Lyons, 2006), but we observe the same stratigraphic trend for Mo/TOC (Figure 2)—suggesting that we are not missing a euxinic interval because of low TOC. Uranium and V on the other hand require less reducing conditions and can be enriched in sediments marked by anoxic but not necessarily euxinic conditions (Tribovillard, Algeo, Lyons, & Riboulleau, 2006; see Supporting Information for a related discussion of V geochemistry and Partin et al., 2013, for additional background on U). Pronounced enrichments for all three metals, combined with the Fe proxy data, point convincingly to dominantly euxinic conditions in the middle Velkerri. The high-end concentrations for Mo and U in this interval are among the largest known for the mid-Proterozoic. Magnitudes of local Mo and U enrichment in euxinic sediments are controlled in part by the spatial extent of euxinia and anoxia in the global ocean (Partin et al., 2013; Reinhard et al., 2013; Scott et al., 2008). As such, these relatively high Mo and U values may mark a transient oxidation event in the ocean–atmosphere system during the mid-Proterozoic. Importantly, other recent, independent studies of Velkerri trace metal and U isotope data have suggested transient, perhaps global-scale marine oxygenation for this time period (Mukherjee & Large, 2016; Yang et al., 2017).

Concentrations for Mo, U, and V above and below the middle interval are at near-crustal levels. Despite evidence for intermittently ferruginous waters in the upper part, Fe_{HR}/Fe_T ratios are generally low in both intervals. Collectively, the trace-metal and Fe speciation results imply at least moderate levels of marine oxygenation locally, and perhaps globally, throughout the Velkerri time of the mid-Proterozoic. Consequently, these samples, for both local and global reasons, are particularly appropriate for our organic geochemical search for eukaryotes.

Consistent with our integrated, conceptual paleoredox model for the Velkerri Formation, manganese (Mn) concentration behaves antithetically to Mo, U, and V, exhibiting low values in the euxinic intervals and high values when the prevailing redox was dominantly oxic (lower Velkerri) or vacillating between ferruginous and oxic conditions (upper Velkerri). These Mn enrichments suggest greater Mn-oxide burial, implying appreciable oxygen periodically in the water column (Calvert & Pedersen, 1993; Froelich et al., 1979). Furthermore, Mn appears to be tracking TIC, which we assume to reflect authigenic Mn-rich carbonate. In this case, the prerequisite for Mn-carbonate precipitation is oxic bottom waters where Mn oxides are trapped in the sediments and redox cycled repeatedly, resulting in dissolved Mn buildup in the subsurface anoxic portions of the pore water profile and subsequent carbon precipitation (Calvert & Pedersen, 1993, 1996).

3.4 | Lipid biomarkers

Our inorganic geochemical framework can yield nuanced information that can resolve longstanding questions about the extent of mid-Proterozoic eukaryotic development, the environmental background, and the nutrient conditions of their early evolution. In this context, we look for possible biomarkers by targeting strata that had appreciably high total organic carbon (TOC) content (>1 wt.%); high

and low Mo concentrations; and facies overall that reflect varying depositional redox environments, including independent suggestions of at least intermittently hospitable oxic conditions in the waters below the surface mixed layer. Consequently, selected samples from Altree-2 core cover most of the Velkerri Formation, ranging from 452 to 1,205 m depth (see Table 1).

Although lipid biomarkers can contribute to a better understanding of mid-Proterozoic ocean chemistry and biology, important analytical self-consistency checks are required to verify syngenicity of the compounds detected. Contamination is a primary concern—from migration of hydrocarbons across a billion or more years of burial history or from oil-based additives used to drill the cores (Grosjean & Logan, 2007). Fortunately, we can screen for this possibility through meticulous methodology designed to identify and prevent contamination (Brocks, 2011; Brocks et al., 2017; Flannery & George, 2014; French et al., 2015; Love et al., 2009; Luo, Hallmann, Xie, Ruan, & Summons, 2015; Pawlowska, Butterfield, & Brocks, 2013; Zumberge et al., 2018).

Saturated and aromatic hydrocarbon fractions, obtained from rock bitumens extracted from inner core portions, were analyzed for this study to generate various parameters such as methylphenanthrene index (MPI-1; Radke & Welte, 1983), as well as various hopane and sterane molecular ratios (Peters, Walters, & Moldowan, 2005; Summons, Powell, & Boreham, 1988). These constraints were used to check for systematic changes in maturity ratios with burial depth to ensure that the bitumen records have not been compromised by high thermal overprints or obvious exogenous hydrocarbon/other contaminant inputs (Table 1). Methylphenanthrene and phenanthrene ratios, in this case using the MPI-1 index, (Table 1) showed systematic increases with increasing burial depth—values began increasing from 0.49 at 725 m (middle Velkerri) to as high as 1.48 at 1205 m (lower Velkerri). This pattern is very similar to previous reports of aromatic hydrocarbons from the same core (Summons et al., 1994). In addition, data for % Rc (vitrinite reflectance calculated from MPI-1) point to a thermal maturity range for these samples spanning from early oil window to within the middle interval of the oil window (Figure 1, Table 1), as independently verified from Rock-Eval data (hydrogen index) and from the alkane biomarker maturity parameters. Cross-checking with ratios of C_{27} hopanes 18α(H)-22,29,30-trisnorneohopane (Ts) and 17α(H)-22,29,30-trisnorhopane (Tm)—where Ts is the most stable thermodynamic configuration, and thus higher values of Ts/(Ts + Tm) represent an increase in thermal maturity (Seifert & Moldowan, 1978)—shows that the alkane and aromatic maturity ratios are self-consistent. A Ts/(Ts + Tm) ratio of 0.59 is observed at 452 m (upper Velkerri); these ratios increase to as high as 0.78 at 852 m. Higher values are generally found in deeper samples, although mineralogy can exert a secondary control on absolute values. Moreover, moretanes (βα–isomers) are thermodynamically less stable than the αβ-hopanes, and the low ratios of C_{30} βα–isomers/αβ–isomers observed (0.06–0.07, Table 1) for the upper and middle Velkerri strata are also consistently uncontaminated hopane signatures from rocks within the oil window.

Across this full gradient in ocean chemistry, as distinguished by inorganic geochemical characteristics, we found no evidence for any C_{27}–C_{30} sterane biomarkers in any samples at levels detectable above our low detection limit using MRM-GC-MS (estimated at <0.1 ppm of total saturated hydrocarbon fraction) in our carefully prepared inner core portions (Figure 3). This observation stands even when we take into account that mid-Proterozoic rock extracts contain unresolvable complex mixtures (UCMs) that can potentially mask small amounts of sterane signal beneath the baseline "hump" (Pawlowska et al., 2013). For example, calibration by addition of nanogramme quantities of deuterated C_{29} sterane standard to the saturated hydrocarbon fractions showed that any diasteranes and/

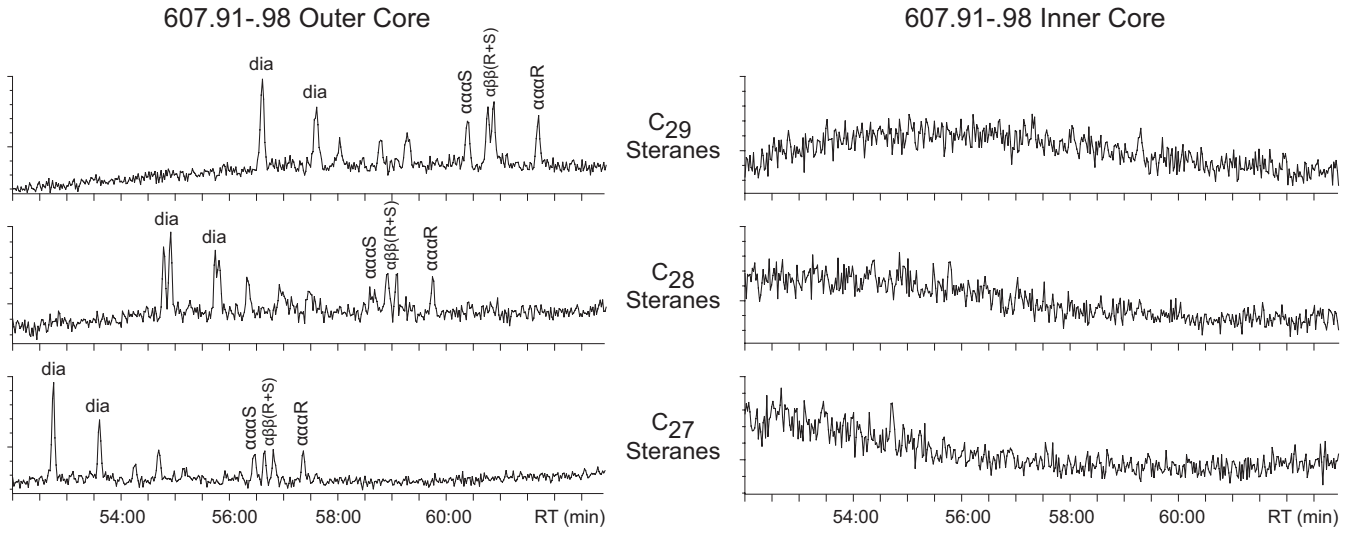

FIGURE 3 A comparison of free (extractable) sterane profiles between the inner and outer core portions of Altree-2 sample (607.91–607.98 m) in the upper Velkerri Fm interval as analyzed by MRM-GC-MS. The outer portion of the core was contaminated by trace quantities of a full suite of younger C_{27}–C_{29} steranes. The inner core, however, is void of any detectable sterane signal compared for equal masses of rock extracted

or regular steranes present must be lower than 0.1 ppm of the total alkane fractions in concentration. Overall, three important self-consistency checks support our finding that eukaryotic sterane biomarkers in these rocks are either absent or present in vanishingly small amounts below detection limits: (a) C_{27-30} regular steranes were also below detection limits in the hydropyrolysates derived from the corresponding kerogen phases for seven pre-extracted rock powders, even though kerogen-bound hopanes were detectable; (b) any detectable amounts of extractable trace steranes were only found in outer exposed core portions, which are more susceptible to contaminant inputs, but were completely absent in the pristine "inner" core portions analyzed separately (Figure 3); and (c) short-chain sterane compounds (in our case, we monitored C_{21+22} steranes using the appropriate MRM-GC-MS transitions), which are commonly found together with the usual C_{27}–C_{30} parent steranes in oil window-mature rocks, were also absent in the inner core extracts and kerogen hydropyrolysates. Additionally, gammacerane, which is the fossil alkane biomarker derived from tetrahymanol which can be synthesized by ciliated protozoans, some low-oxygen-adapted unicellular eukaryotes as well as some bacteria (Takashita et al., 2017), is only found in trace amounts relative to hopanes in two samples and is below detection limits in all the others (Table 1).

In addition to the lack of discernible steranes, patterns of linear and branched alkanes (mostly in the C_{13}–C_{24} range for *n*-alkanes and methylalkanes in total ion chromatograms), as well as identification of robust hopane signals using MRM-GC-MS detection for both the bitumen and kerogen products (Figures 4 and 5), suggest a bacterially dominated ecology that drove primary productivity as found previously from analyses of extractable bitumen from middle Velkerri Formation black shales from the Walton-2 core (Flannery & George, 2014). Analyses of oil inclusions from the Bessie Creek Sandstone underlying the Velkerri Formation (which is the most likely source

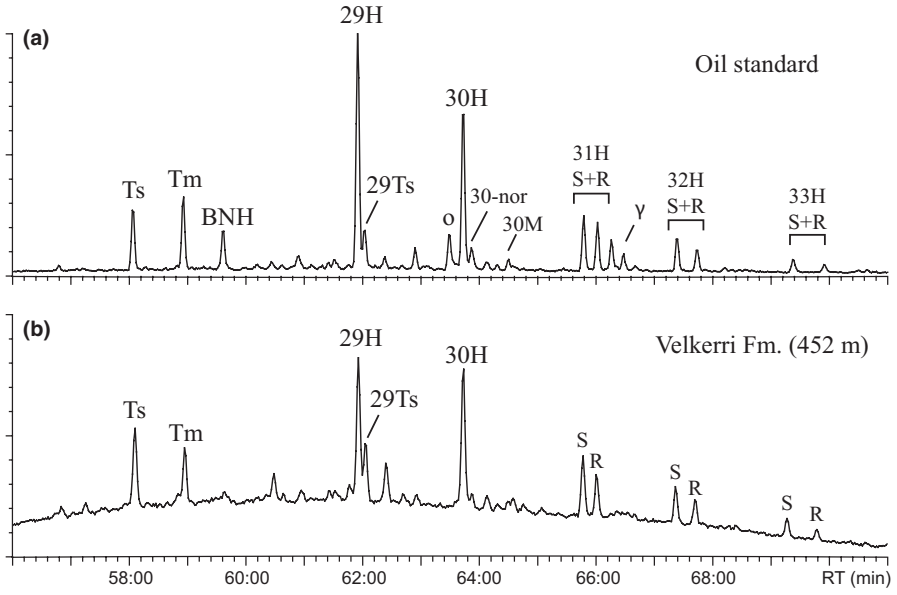

FIGURE 4 Comparison of C_{27}–C_{33} hopane distributions from MRM-GCMS of saturated hydrocarbon fractions for (a) Phanerozoic oil standard and (b) Altree-2 rock bitumen extract (ca. 452 m depth) from the upper member of the Velkerri Fm. See Table 1 for peak assignments

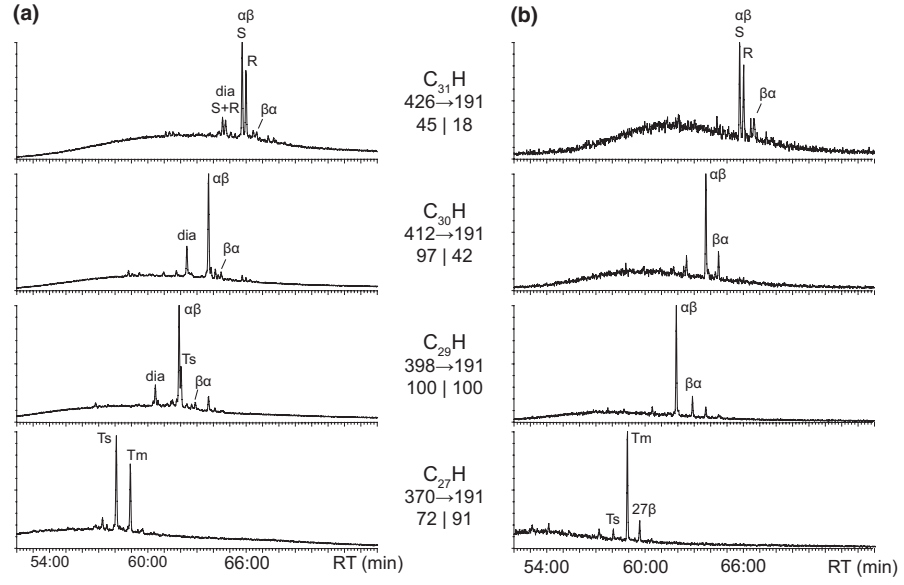

FIGURE 5 Comparison of free (extractable) and kerogen-bound C_{27}–C_{31} hopanes from MRM-GCMS of saturated hydrocarbon fractions for (a) solvent-extractable bitumen and (b) kerogen hydropyrolysate of Altree-2 sample from ca. 452 m depth. See Table 1 for peak assignments. MRM parent/daughter transitions and relative abundances are also shown. The kerogen-bound hopanes exhibit a slightly less mature diasteroisomeric distribution than the free hopanes due to steric protection through binding in the kerogen matrix (Love et al., 1995), which is the classic ancient biomarker pattern for rocks of all ages and a positive test for syngenicity of the hopane series in these rocks

rock) revealed a broad range biomarkers derived mainly from bacteria but either lacking or having only trace quantities of eukaryotic sterane biomarkers (Dutkiewicz, Volk, Ridley, & George, 2003). Overall, the geochemistry of the oil inclusions, in terms of the major hydrocarbon constituents, is very similar to the bitumen and source rocks observed from the Roper Group (Flannery & George, 2014; Volk, Dutkiewicz, George, & Ridley, 2003; Volk, George, Dutkiewicz, & Ridley, 2005). Further, since other polycyclic biomarker alkanes were preserved in these rocks (such as tricyclic terpanes and hopanes), the absence of sterane signal is not due to poor biomarker preservation arising from structural modification or destruction due to thermal cracking during burial maturation, consistent with the low thermal grade of the strata as already demonstrated.

Not only were regular steranes absent in the euxinic interval, but they were also not detected in the relatively more oxic facies, suggesting that (steroid-synthesizing) eukaryotes were not ecologically widespread and abundant in such distal shelf marine settings during this mid-Proterozoic interval—in contrast to the later Proterozoic. Previous models have asserted that low nutrient availability and associated deficiencies in oxygen may have throttled early diversity and abundances of eukaryotes (Anbar & Knoll, 2002; Javaux, Knoll, & Walter, 2001; Lyons et al., 2014; Reinhard et al., 2013). Alternatively, a taphonomic bias effect has been proposed for low preservation potential of steroids in mid-Proterozoic rocks (Pawlowska et al., 2013), a hypothetical mechanism termed the "mat-seal effect" in which enhanced microbial reworking of steroid lipids deposited on the surface of benthic microbial mats was proposed to preferentially deplete sedimentary steroid compounds in the extractable bitumen phase. In our study, we find no evidence for (a) short sterane compounds (C_{21+22} steranes) with partially degraded side-chains in the rock bitumens, or (b) or any bound sterane compounds covalently linked within the (insoluble) kerogen phase which would have been sequestered early in the depositional history. It has been shown previously from a range of modern aquatic environments that kerogen formation commences very early during diagenesis, beginning in the water column and resulting in appreciable sequestration of biolipids into an insoluble macromolecular organic phase that is not readily biodegradable (Farrimond et al., 2003). Since the macromolecular host matrix protects the bound molecular constituents from microbial degradation, the complete lack of any free or kerogen-bound sterane biomarkers detected in Velkerri Fm. rocks shown here suggests that the dearth of regular steranes is unlikely to be a consequence of a "mat-seal" taphonomic bias operating against preservation of ancient steroid biomarkers.

Full scan GC-MS analysis of aromatic fractions from the rock bitumens also revealed no discernible aromatic carotenoid biomarkers derived from anoxygenic photosynthetic bacteria, such as Chlorobi, in 133 and 134 Da mass chromatograms. Despite other series of polyaromatic hydrocarbons being abundant, both the 2,3,6- and 2,3,4-trimethyl-substituted aryl isoprenoidal series were below our detection limit estimated at 1 ppm of the total mass of aromatic hydrocarbons for individual compounds. Abundant aromatic carotenoid biomarkers for both green and purple sulfur bacteria were detected previously in rocks of the 1.64 Ga Barney Creek Formation, also from the McArthur Basin (Brocks et al., 2005). In contrast, the Velkerri Formation shows no detectable aryl isoprenoids and C_{40} parent carotenoid markers for anoxygenic phototrophic bacteria, which suggests that photic zone euxinia was not commonly sustained in the depositional environment. Further, since the water column depth for Velkerri Fm. strata, deposited in deep marine settings on the outer slope and more distal, is likely to have been significantly deeper than photic zone water depths (typically down to ca. 100 m), then proliferation of photosynthetic benthic mats on the seafloor would be likely unsustainable due to low light level restrictions.

With our new results, we can comfortably assert that the absence of diagnostic biomarkers for eukaryotic organisms is not a product of locally inhospitable conditions due to a continuous absence of oxygen in the bottom waters and a corresponding persistence of anoxia or euxinia. The suggestion, then, is that the environment of the Velkerri Formation may have been, if anything, more favorable than many mid-Proterozoic settings. Specifically, the Velkerri was likely marked by at least episodically hospitable waters during an interval in Earth history more generally characterized by delayed eukaryotic proliferation in more prominently inhospitable oceans. In other words, the Velkerri Formation provides a special if not unique environmental window to sample the global evolutionary state of complex life—free of local redox bias.

Molecular clock studies (Gold, Caron, Fournier, & Summons, 2017) predict that sterol synthesis evolved early in eukaryotic evolution significantly prior to the diversification of crown group eukaryotes and that the last eukaryotic common ancestor LECA was probably capable of making sterols (Desmond & Gribaldo, 2009). In support of this, bacterially derived steroids with methylation preserved at C-4 (Wei, Yin, & Welander, 2016) have been reported in immature rocks from ca. 1.64 Ga Barney Creek Formation (Brocks et al., 2005) showing that steroid synthesis significantly predates the 1.3–1.4 Ga Roper Group. A fundamental conclusion of our study then is that eukaryotes did not make significant contributions to the sedimentary organic matter deposited in the McArthur Basin, as gauged from biomarker abundance patterns, suggesting that eukaryotes were not abundant marine primary producers during this interval of the mid-Proterozoic. One important caveat is that low-oxygen-adapted eukaryotes which did not possess sterols may have been part of the community structure, since a few anaerobic protists have recently been shown to lack either sterols or tetrahymanol in their cell membranes (Takashita et al., 2017). Both a low abundance of microbial eukaryotes relative to bacteria and the possibility of adapted eukaryotic protists that did not make steroids or tetrahymanol can potentially reconcile the finding of eukaryotic microfossils in Roper Group strata (Javaux, Knoll, & Walter, 2004) but no detectable record of established eukaryotic biomarkers.

A recent consensus has emerged from careful analysis of low maturity ancient sedimentary rocks that C_{27}–C_{30} steranes, biomarkers sourced from eukaryotes, are below detection in rock bitumens for mid-Proterozoic strata and more generally in rocks older than ca. 800 Ma (Blumenberg, Thiel, Riegel, Kah, & Reitner, 2012; Brocks

et al., 2005, 2015, 2017; Flannery & George, 2014; French et al., 2015; Isson et al., 2018; Luo et al., 2015; Pawlowska et al., 2013). Indeed, the oldest robust reports of ancient steranes derive from rocks of the Chuar Group and Visingsö Group (700–800 Ma) using the high sensitivity of MRM-GC-MS for biomarker detection (Brocks et al., 2015, 2017). In contrast, abundant hopanes derived from diverse bacterial source are ubiquitous in immature rocks as far back as 1.64 Ga (Brocks et al., 2005). The most parsimonious interpretation of the lack of detectable steranes in our view is that aerobic eukaryotes did not become ecologically widespread and abundant in the global oceans until well into the Neoproterozoic era (Brocks et al., 2017) and that source biota in mid-Proterozoic and older oceans were dominated by bacteria (Brocks et al., 2005, 2017; Flannery & George, 2014; Isson et al., 2018; Luo et al., 2015). A recent molecular clock analysis (Gibson et al., 2017) predicts that photosynthesis did not actually emerge in Eukarya until ca. 1.25 Ga, and this could help explain the bacterial ecological dominance of Roper Group biomarker assemblages, although the divergence time uncertainties for such estimates can be large and this innovation does not coincide with the ubiquity of eukaryotic steranes in ancient rocks being delayed until ca. 800 Ma and younger, as described above.

Previous microfossil studies indicate only a modest Mesoproterozoic eukaryote diversity as gauged from acritarchs (Beghin et al., 2017; Javaux et al., 2004), even from settings interpreted as oxic in the Mesoproterozoic ocean (Sergeev, Knoll, Vorob'eva, & Sergeeva, 2016; Sperling et al., 2014). Furthermore, the apparent disparity between some occurrences of Mesoproterozoic eukaryotic acritarchs yet no detectable record of regular steranes appears to continue till 1.0 Ga in the Malgin Formation of the Siberian Platform (Suslova, Parfenova, Saraev, & Nagovitsyn, 2017), while thermally immature rocks from the 1.1 Ga Atar Group were also shown to be devoid of steroid biomarkers (Blumenberg et al., 2012). While microfossil analysis is the most sensitive and appropriate approach for assessing the first appearance of eukaryotic cells in ancient sedimentary rocks, discernible acritarch microfossils typically represent only a small mass fraction of the total ancient sedimentary organic matter (mainly amorphous kerogen) and thus it is difficult to quantify the eukaryotic contributions without lipid biomarker source input constraints. Insights from a combination of microfossil and biomarker approaches in the studies of Proterozoic geobiology are hence useful and complementary.

4 | CONCLUSIONS

Iron and trace-metal data from the Velkerri Formation reveal that there was more apparent temporal variability in the marine redox conditions, at least locally and perhaps globally, during the mid-Proterozoic than was previously recognized through analysis of the same interval (Kendall et al., 2009; Mukherjee & Large, 2016; Shen, Canfield, & Knoll, 2002; Shen et al., 2003; Yang et al., 2017). Overall, the system appears to have evolved from one that was dominantly oxic during deposition of the lower Velkerri Formation to euxinic in the middle Velkerri. More specifically, the middle unit is marked by evidence for a transient period of euxinia bracketed by evidence for more persistent water column sulfide prior to the deposition of the upper Velkerri, as supported by the combined Fe and Mo data. The upper Velkerri Formation shows an intriguing combination of low trace-metal abundances but numerous Fe speciation data suggesting frequent ferruginous but not euxinic deposition—with other Fe speciation data that are more reasonably attributed to oxic conditions. The lack of U and V enrichment places possible constraints on the limited duration of the anoxic conditions—and the relative rates of U and V versus Fe enrichment—and the possibility of V and U remobilization under conditions of rapid redox variability (and subsequent oxic overprints specifically). The Fe signatures of ferruginous conditions, by contrast, could be retained even if reduced Fe phases were oxidized. The most likely scenario for the upper interval is one of oscillatory redox between oxic and anoxic marine deposition.

A recent view of the mid-Proterozoic ocean redox structure was presented in Planavsky et al. (2011) and Poulton and Canfield (2011), which suggests a dominantly ferruginous deep ocean with euxinia limited to productive margins (see also Reinhard et al., 2013; as reviewed in Lyons et al., 2014). Our data—specifically comparatively high Mo contents in the middle euxinic interval and suggestions from the Fe speciation data for at least intermittently oxic conditions above and below, perhaps at some appreciable water depth given the fine-grained nature of the sediments—suggest redox variability and an interval of relatively oxic marine conditions in the mid-Proterozoic. The depth, lateral extent, and concentrations of marine oxygenation are difficult to constrain and in no way unambiguously demand widespread oxygenation during this interval. These inferred conditions for the Velkerri Formation do, however, make it a particularly attractive target in our search for eukaryotic biosignatures—within a framework of both local and global redox and implied nutrient controls. Moreover, we should be able to infer qualitatively variations in productivity and organic matter preservation across local redox gradients, if those local controls dominated the eukaryotic signal strength. In other words, we looked for eukaryotic signals in facies expected to favor their production (oxic) and preservation (anoxic)—recognizing that anoxic bottom waters can record (with strong fidelity) eukaryotic production in shallow, overlying oxic waters. At the same time, proximal deeper anoxic waters can challenge shallow eukaryotic life through upward mixing of those waters (Hardisty et al., 2017).

Despite our careful, independent consideration of primary redox controls, biomarker data across the three intervals of the Velkerri Formation show no clear evidence for the presence of the regular sterane compounds that are considered diagnostic of eukaryotic life, even in strata with appreciable TOC and suggestions of oxic deposition. In addition, there are no significant detectable levels of aromatic carotenoid biomarkers for green and purple sulfur bacteria; thus, substantial anoxygenic photosynthesis could not have been supported as a major mode of primary production at least in this setting at this time (Johnston et al., 2009). The lack of aryl isoprenoids and C_{40}

parent carotenoid markers for anoxygenic phototrophic bacteria in the Velkerri Formation contrasts biomarker evidence for green and purple sulfur bacteria found in the older Barney Creek Formation (Brocks et al., 2005). We are left with the conclusion that photic zone euxinia, if present, was perhaps of relatively limited extent during deposition of the Velkerri Formation even though deeper euxinic conditions were relatively widespread compared to the modern record (Reinhard et al., 2013). While we are providing only one snapshot of the mid-Proterozoic world, it also raises doubts as to whether euxinia was shallow and abundant enough to support appreciable anoxygenic primary production via sulfide oxidation—particularly in open marine settings. Overall, the absence of eukaryotic biomarker signals in our samples—despite our careful search within a paleoenvironmental context informed by iron mineral and trace element geochemistry—suggests that other controls such as synergistic long-term nutrient and ecological factors may have held complex eukaryotic life at bay pending the profound environmental changes that marked the later Proterozoic.

ACKNOWLEDGMENTS

Funding was provided by the Earth-Life Transitions and FESD programs of the U.S. National Science Foundation and the NASA Astrobiology Institute under Cooperative Agreement No. NNA15BB03A issued through the Science Mission Directorate. GDL thanks the Agouron Institute for the Autospec GC-MS instrument at UCR. Many thanks to the people who helped with laboratory work, analysis, and discussion: Dalton Hardisty, Emily Haddad, Rosemarie Bisquera, Konstantin Choumiline, Petra Schoon, Alexandria Ruiz, Laura Wehrmann, Natascha Riedinger, and Michael Dahl.

CONFLICT OF INTEREST

The authors declare no conflicting interests, financial or otherwise.

ORCID

Gordon D. Love https://orcid.org/0000-0002-6516-014X

REFERENCES

Abbott, S. T., & Sweet, I. P. (2000). Tectonic control on third-order sequences in a siliciclastic ramp-style basin: An example from the Roper Superbasin (Mesoproterozoic), northern Australia. *Australian Journal of Earth Sciences*, *47*, 637–657. https://doi.org/10.1046/j.1440-0952.2000.00795.x

Algeo, T. J., & Lyons, T. W. (2006). Mo–total organic carbon covariation in modern anoxic marine environments: Implications for analysis of paleoredox and paleohydrographic conditions. *Paleoceanography*, *21*, PA1016. https://doi.org/10.1029/2004pa001112

Anbar, A. D., & Knoll, A. H. (2002). Proterozoic ocean chemistry and evolution: A bioinorganic bridge? *Science*, *297*, 1137–1142. https://doi.org/10.1126/science.1069651

Beghin, J., Storme, J.-Y., Blanpied, C., Gueneli, N., Brocks, J. J., Poulton, S. W., & Javaux, E. J. (2017). Microfossils from the late Mesoproterozoic – Early Neoproterozoic Atar/El Mreiti Group, Taoudeni Basin, Mauritania, northwestern Africa. *Precambrian Research*, *291*, 63–82. https://doi.org/10.1016/j.precamres.2017.01.009

Bekker, A., Holland, H., Wang, P.-L., Rumble, D., Stein, H., Hannah, J., … Beukes, N. (2004). Dating the rise of atmospheric oxygen. *Nature*, *427*, 117–120. https://doi.org/10.1038/nature02260

Blumenberg, M., Thiel, V., Riegel, W., Kah, L. C., & Reitner, J. (2012). Biomarkers of black shales formed by microbial mats, Late Mesoproterozoic (1.1 Ga) Taoudeni Basin, Mauritania. *Precambrian Research*, *196–197*, 113–127. https://doi.org/10.1016/j.precamres.2011.11.010

Brasier, M. D., & Lindsay, J. F. (1998). A billion years of environmental stability and the emergence of eukaryotes: New data from northern Australia. *Geology*, *26*, 555–558. https://doi.org/10.1130/0091-7613(1998)026<0555:ABYOES>2.3.CO;2

Brocks, J. J. (2011). Millimeter-scale concentration gradients of hydrocarbons in Archean shales: Live-oil escape or fingerprint of contamination? *Geochimica et Cosmochimica Acta*, *75*, 3196–3213. https://doi.org/10.1016/j.gca.2011.03.014

Brocks, J. J., Jarrett, A. J. M., Sirantoine, E., Hallmann, C., Hoshino, Y., Liyanage, T. (2017). The rise of algae in Cryogenian oceans and the emergence of animals. *Nature*, *548*, 578–581. https://doi.org/10.1038/nature23457

Brocks, J. J., Jarrett, A. J., Sirantoine, E., Kenig, F., Moczydlowska, M., Porter, S., & Hope, J. (2015). Early sponges and toxic protists: Possible sources of cryostane, an age diagnostic biomarker antedating Sturtian Snowball Earth. *Geobiology*, *14*, 129–149.

Brocks, J. J., Love, G. D., Summons, R. E., Knoll, A. H., Logan, G. A., & Bowden, S. A. (2005). Biomarker evidence for green and purple sulphur bacteria in a stratified Palaeoproterozoic sea. *Nature*, *437*, 866–870. https://doi.org/10.1038/nature04068

Buick, R., Des Marais, D. J., & Knoll, A. H. (1995). Stable isotopic compositions of carbonates from the Mesoproterozoic Bangemall group, northwestern Australia. *Chemical Geology*, *123*, 153–171. https://doi.org/10.1016/0009-2541(95)00049-R

Calvert, S. E., & Pedersen, T. F. (1993). Geochemistry of recent oxic and anoxic marine sediments: Implications for the geological record. *Marine Geology*, *113*, 67–88. https://doi.org/10.1016/0025-3227(93)90150-T

Calvert, S. E., & Pedersen, T. F. (1996). Sedimentary geochemistry of manganese; implications for the environment of formation of manganiferous black shales. *Economic Geology*, *91*, 36–47. https://doi.org/10.2113/gsecongeo.91.1.36

Canfield, D. E. (1998). A new model for Proterozoic ocean chemistry. *Nature*, *396*, 450–453. https://doi.org/10.1038/24839

Canfield, D. E., Farquhar, J., & Zerkle, A. L. (2010). High isotope fractionations during sulfate reduction in a low-sulfate euxinic ocean analog. *Geology*, *38*, 415–418. https://doi.org/10.1130/G30723.1

Canfield, D. E., Raiswell, R., & Bottrell, S. H. (1992). The reactivity of sedimentary iron minerals toward sulfide. *American Journal of Science*, *292*, 659–683. https://doi.org/10.2475/ajs.292.9.659

Canfield, D. E., Raiswell, R., Westrich, J. T., Reaves, C. M., & Berner, R. A. (1986). The use of chromium reduction in the analysis of reduced inorganic sulfur in sediments and shales. *Chemical Geology*, *54*, 149–155. https://doi.org/10.1016/0009-2541(86)90078-1

Crick, I. H. (1992). Petrological and maturation characteristics of organic matter from the middle Proterozoic McArthur Basin, Australia. *Australian Journal of Earth Sciences*, *39*, 501–519. https://doi.org/10.1080/08120099208728042

Derry, L. A. (2015). Causes and consequences of mid-Proterozoic anoxia. *Geophysical Research Letters*, *42*, 8538–8546. https://doi.org/10.1002/2015GL065333

Desmond, E., & Gribaldo, S. (2009). Phylogenomics of sterol synthesis: Insights into the origin, evolution, and diversity of a key eukaryotic feature. *Genome Biology and Evolution*, *1*, 364–381. https://doi.org/10.1093/gbe/evp036

Dutkiewicz, A., Volk, H., Ridley, J., & George, S. C. (2003). Biomarkers, brines, and oil in the Mesoproterozoic, Roper Superbasin, Australia. *Geology*, *31*, 981–984. https://doi.org/10.1130/G19754.1

Farrimond, P., Love, G. D., Bishop, A. N., Innes, H. E., Watson, D. F., & Snape, C. E. (2003). Evidence for the rapid incorporation of hopanoids into kerogen. *Geochimica et Cosmochimica Acta*, *67*, 1383–1394. https://doi.org/10.1016/S0016-7037(02)01287-5

Flannery, E. N., & George, S. C. (2014). Assessing the syngeneity and indigeneity of hydrocarbons in the ~1.4 Ga Velkerri Formation, McArthur Basin, using slice experiments. *Organic Geochemistry*, *77*, 115–125. https://doi.org/10.1016/j.orggeochem.2014.10.008

French, K. L., Hallmann, C., Hope, J. M., Schoon, P. L., Zumberge, J. A., Hoshiono, Y., … Summons, R. E. (2015). Reappraisal of hydrocarbon biomarkers in Archean rocks. *Proceedings of the National Academy of Sciences*, *112*(19), 5915–5920. https://doi.org/10.1073/pnas.1419563112

Froelich, P. N., Klinkhammer, G. P., Bender, M. L., Luedtke, N. A., Heath, G. R., Cullen, D., … Maynard, V. (1979). Early oxidation of organic matter in pelagic sediments of the eastern equatorial Atlantic: Suboxic diagenesis. *Geochimica et Cosmochimica Acta*, *43*, 1075–1090. https://doi.org/10.1016/0016-7037(79)90095-4

Gibson, T. M., Shih, P. M., Cumming, V. M., Fischer, W. W., Crockford, P. W., Hodgskiss, M. S. W., … Halverson, G. P. (2017). Precise age of *Bangiomorpha pubescens* dates the origin of eukaryotic photosynthesis. *Geology*, *46*, 135–138.

Gold, D. A., Caron, A., Fournier, G. P., & Summons, R. E. (2017). Paleoproterozoic sterol biosynthesis and the rise of oxygen. *Nature*, *543*, 420–423. https://doi.org/10.1038/nature21412

Grosjean, E., & Logan, G. A. (2007). Incorporation of organic contaminants into geochemical samples and an assessment of potential sources: Examples from Geoscience Australia marine survey S282. *Organic Geochemistry*, *38*, 853–869. https://doi.org/10.1016/j.orggeochem.2006.12.013

Hardisty, D. S., Lu, Z., Bekker, A., Diamond, C. W., Gill, B. C., Jiang, G., … Lyons, T. W. (2017). Perspectives on Proterozoic surface ocean redox from iodine contents in ancient and recent carbonate. *Earth and Planetary Science Letters*, *463*, 159–170. https://doi.org/10.1016/j.epsl.2017.01.032

Isson, T. T., Love, G. D., Dupont, C. L., Reinhard, C. T., Zumberge, J. A., Asael, D., … Planavsky, N. J. (2018). Tracking the rise of eukaryotes to ecological dominance with zinc isotopes. *Geobiology*, *16*, 341–352. https://doi.org/10.1111/gbi.12289

Jackson, M. J., Powell, T. G., Summons, R. E., & Sweet, I. P. (1986). Hydrocarbon shows and petroleum source rocks in sediments as old as 1.7×10^9 years. *Nature*, *322*, 727–729. https://doi.org/10.1038/322727a0

Jackson, M. J., & Raiswell, R. (1991). Sedimentology and carbon-sulphur geochemistry of the Velkerri Formation, a mid-Proterozoic potential oil source in northern Australia. *Precambrian Research*, *54*, 81–108. https://doi.org/10.1016/0301-9268(91)90070-Q

Jackson, M. J., Sweet, I. P., Page, R. W., & Bradshaw, B. E. (1999). The South Nicholson and Roper Groups: Evidence for the early Mesoproterozoic Roper superbasin. In B. E. Bradshaw & D. L. Scott (Eds.), *Integrated basin analysis of the Isa superbasin using seismic, well-log, and geopotential data: An evaluation of the economic potential of the Northern Lawn Hill Platform*. Canberra, ACT: Australian Geological Survey Organisation Record 19.

Jackson, M. J., Sweet, I., & Powell, T. G. (1988). Petroleum geology and geochemistry of the Middle Proterozoic, McArthur Basin, Northern Australia. I: Petroleum potential. *Aust. Petrol. Explor. Assoc. J*, *28*, 283.

Javaux, E. J., Knoll, A. H., & Walter, M. R. (2001). Morphological and ecological complexity in early eukaryotic ecosystems. *Nature*, *412*, 66–69. https://doi.org/10.1038/35083562

Javaux, E. J., Knoll, A. H., & Walter, M. R. (2004). TEM evidence for eukaryotic diversity in mid-Proterozoic oceans. *Geobiology*, *2*, 121–133. https://doi.org/10.1111/j.1472-4677.2004.00027.x

Johnston, D. T., Wolfe-Simon, F., Pearson, A., & Knoll, A. H. (2009). Anoxygenic photosynthesis modulated Proterozoic oxygen and sustained Earth's middle age. *Proceedings of the National Academy of Sciences*, *106*, 16925–16929. https://doi.org/10.1073/pnas.0909248106

Kah, L. C., Lyons, T. W., & Frank, T. D. (2004). Low marine sulphate and protracted oxygenation of the Proterozoic biosphere. *Nature*, *431*, 834–838. https://doi.org/10.1038/nature02974

Kendall, B., Creaser, R. A., Gordon, G. W., & Anbar, A. D. (2009). Re–Os and Mo isotope systematics of black shales from the Middle Proterozoic Velkerri and Wollogorang formations, McArthur Basin, northern Australia. *Geochimica et Cosmochimica Acta*, *73*, 2534–2558. https://doi.org/10.1016/j.gca.2009.02.013

Knoll, A. H., Javaux, E. J., Hewitt, D., & Cohen, P. (2006). Eukaryotic organisms in Proterozoic oceans. *Philosophical Transactions of the Royal Society B: Biological Sciences*, *361*, 1023–1038. https://doi.org/10.1098/rstb.2006.1843

Laakso, T. A., & Schrag, D. P. (2017). A theory of atmospheric oxygen. *Geobiology*, *15*(3), 366–384. https://doi.org/10.1111/gbi.12230

Love, G. D., Grosjean, E., Stalvies, C., Fike, D. A., Grotzinger, J. P., Bradley, A. S., … Summons, R. E. (2009). Fossil steroids record the appearance of Demospongiae during the Cryogenian period. *Nature*, *457*, 718–722. https://doi.org/10.1038/nature07673

Love, G. D., Snape, C. E., Carr, A. D., & Houghton, R. C. (1995). Release of covalently-bound biomarkers in high yields from kerogen via catalytic hydropyrolysis. *Organic Geochemistry*, *23*, 981–986. https://doi.org/10.1016/0146-6380(95)00075-5

Luo, G., Hallmann, C., Xie, S., Ruan, X., & Summons, R. E. (2015). Comparative microbial diversity and redox environments of black shale and stromatolite facies in the Mesoproterozoic Xiamaling Formation. *Geochimica et Cosmochimica Acta*, *151*, 150–167. https://doi.org/10.1016/j.gca.2014.12.022

Luo, G., Ono, S., Beukes, N. J., Wang, D. T., Xie, S., & Summons, R. E. (2016). Rapid oxygenation of Earth's atmosphere 2.33 billion years ago. *Science Advances*, *2*, e1600134. https://doi.org/10.1126/sciadv.1600134

Lyons, T. W. (1997). Sulfur isotopic trends and pathways of iron sulfide formation in upper Holocene sediments of the anoxic Black Sea. *Geochimica et Cosmochimica Acta*, *61*, 3367–3382. https://doi.org/10.1016/S0016-7037(97)00174-9

Lyons, T. W., Reinhard, C. T., & Planavsky, N. J. (2014). The rise of oxygen in Earth/'s early ocean and atmosphere. *Nature*, *506*, 307–315. https://doi.org/10.1038/nature13068

Lyons, T. W., Reinhard, C. T., & Scott, C. (2009). Redox redux. *Geobiology*, *7*, 489–494. https://doi.org/10.1111/j.1472-4669.2009.00222.x

Lyons, T. W., & Severmann, S. (2006). A critical look at iron paleoredox proxies: New insights from modern euxinic marine basins. *Geochimica et Cosmochimica Acta*, *70*, 5698–5722. https://doi.org/10.1016/j.gca.2006.08.021

Muir, M., Donnelly, T., Wilkins, R., & Armstrong, K. (1985). Stable isotope, petrological, and fluid inclusion studies of minor mineral deposits from the McArthur Basin: Implications for the genesis of some sediment-hosted base metal mineralization from the Northern Territory. *Australian Journal of Earth Sciences*, *32*, 239–260. https://doi.org/10.1080/08120098508729328

Mukherjee, I., & Large, R. R. (2016). Pyrite trace element chemistry of the Velkerri Formation, Roper Group, McArthur Basin: Evidence for atmospheric oxygenation during the Boring Billion. *Precambrian Research*, *281*, 13–26. https://doi.org/10.1016/j.precamres.2016.05.003

Och, L. M., & Shields-Zhou, G. A. (2012). The Neoproterozoic oxygenation event: Environmental perturbations and biogeochemical cycling. *Earth-Science Reviews*, *110*, 26–57. https://doi.org/10.1016/j.earscirev.2011.09.004

Parfrey, L. W., Lahr, D. J. G., Knoll, A. H., & Katz, L. A. (2011). Estimating the timing of early eukaryotic diversification with multigene molecular clocks. *Proceedings of the National Academy of Sciences*, *108*, 13624–13629. https://doi.org/10.1073/pnas.1110633108

Partin, C. A., Bekker, A., Planavsky, N. J., Scott, C. T., Gill, B. C., Li, C., … Lyons, T. W. (2013). Large-scale fluctuations in Precambrian atmospheric and oceanic oxygen levels from the record of U in shales. *Earth and Planetary Science Letters*, *369–370*, 284–293. https://doi.org/10.1016/j.epsl.2013.03.031

Pawlowska, M. M., Butterfield, N. J., & Brocks, J. J. (2013). Lipid taphonomy in the Proterozoic and the effect of microbial mats on biomarker preservation. *Geology*, *41*, 103–106. https://doi.org/10.1130/G33525.1

Peters, K. E., Walters, C. C., & Moldowan, J. M. (2005). *The biomarker guide*. Cambridge, UK: Cambridge University Press.

Planavsky, N. J., McGoldrick, P., Scott, C. T., Li, C., Reinhard, C. T., Kelly, A. E., … Lyons, T. W. (2011). Widespread iron-rich conditions in the mid-Proterozoic ocean. *Nature*, *477*, 448–451. https://doi.org/10.1038/nature10327

Poulton, S. W., & Canfield, D. E. (2005). Development of a sequential extraction procedure for iron: Implications for iron partitioning in continentally derived particulates. *Chemical Geology*, *214*, 209–221. https://doi.org/10.1016/j.chemgeo.2004.09.003

Poulton, S. W., & Canfield, D. E. (2011). Ferruginous conditions: A dominant feature of the ocean through Earth's history. *Elements*, *7*, 107–112. https://doi.org/10.2113/gselements.7.2.107

Radke, M., & Welte, D. (1983). The methylphenanthrene index (MPI): A maturity parameter based on aromatic hydrocarbons. In M. Bjorøy et al. (Eds.), *Advances in organic geochemistry 1981* (pp. 504–512). Chichester, UK: Wiley.

Raiswell, R., Buckley, F., Berner, R. A., & Anderson, T. (1988). Degree of pyritization of iron as a paleoenvironmental indicator of bottom-water oxygenation. *Journal of Sedimentary Research*, *58*(5), 812–819.

Raiswell, R., & Canfield, D. E. (1998). Sources of iron for pyrite formation in marine sediments. *American Journal of Science*, *298*, 219–245. https://doi.org/10.2475/ajs.298.3.219

Reinhard, C. T., Planavsky, N. J., Gill, B. C., Ozaki, K., Robbins, L. J., Lyons, T. W., … Konhauser, K. O. (2016). Evolution of the global phosphorus cycle. *Nature*, *541*, 386–389.

Reinhard, C. T., Planavsky, N. J., Robbins, L. J., Partin, C. A., Gill, B. C., Lalonde, S. V., … Lyons, T. W. (2013). Proterozoic ocean redox and biogeochemical stasis. *Proceedings of the National Academy of Sciences*, *110*, 5357–5362. https://doi.org/10.1073/pnas.1208622110

Scott, C., & Lyons, T. W. (2012). Contrasting molybdenum cycling and isotopic properties in euxinic versus non-euxinic sediments and sedimentary rocks: Refining the paleoproxies. *Chemical Geology*, *324*, 19–27. https://doi.org/10.1016/j.chemgeo.2012.05.012

Scott, C., Lyons, T. W., Bekker, A., Shen, Y., Poulton, S. W., Chu, X., & Anbar, A. D. (2008). Tracing the stepwise oxygenation of the Proterozoic ocean. *Nature*, *452*, 456–459. https://doi.org/10.1038/nature06811

Seifert, W. K., & Moldowan, J. M. (1978). Applications of steranes, terpanes and monoaromatics to the maturation, migration and source of crude oils. *Geochimica et Cosmochimica Acta*, *42*, 77–95. https://doi.org/10.1016/0016-7037(78)90219-3

Sergeev, V. N., Knoll, A. H., Vorob'eva, N. G., & Sergeeva, N. D. (2016). Microfossils from the lower Mesoproterozoic Kaltasy Formation, East European Platform. *Precambrian Research*, *278*, 87–107. https://doi.org/10.1016/j.precamres.2016.03.015

Shen, Y., Canfield, D. E., & Knoll, A. H. (2002). Middle Proterozoic ocean chemistry: Evidence from the McArthur Basin, northern Australia. *American Journal of Science*, *302*, 81–109. https://doi.org/10.2475/ajs.302.2.81

Shen, Y., Knoll, A. H., & Walter, M. R. (2003). Evidence for low sulphate and anoxia in a mid-Proterozoic marine basin. *Nature*, *423*, 632–635. https://doi.org/10.1038/nature01651

Sperling, E. A., Rooney, A. D., Hays, L., Sergeev, V. N., Vorob'eva, N. G., Shergeeva, N. D., … Knoll, A. H. (2014). Redox heterogeneity of subsurface waters in the Mesoproterozoic ocean. *Geobiology*, *12*, 373–386. https://doi.org/10.1111/gbi.12091

Summons, R. E., Powell, T. G., & Boreham, C. J. (1988). Petroleum geology and geochemistry of the Middle Proterozoic McArthur Basin, Northern Australia: III. Composition of extractable hydrocarbons. *Geochimica et Cosmochimica Acta*, *52*, 1747–1763. https://doi.org/10.1016/0016-7037(88)90001-4

Summons, R. E., Taylor, D., & Boreham, C. (1994). Geochemical tools for evaluating petroleum generation in the Middle Proterozoic sediments of the McArthur Basin, Northern Territory, Australia. *Australian Petroleum Exploration Association Journal*, *34*, 692.

Suslova, E. A., Parfenova, T. M., Saraev, S. V., & Nagovitsyn, K. E. (2017). Organic geochemistry of rocks of the Mesoproterozoic Malgin Formation and their depositional environments (southeastern Siberian Platform). *Russian Geology and Geophysics*, *58*, 516–528. https://doi.org/10.1016/j.rgg.2016.09.027

Takashita, K., Chikarisha, Y., Tanifuji, G., Ohkouchi, N., Hashimoto, T., Fujikara, K., & Roger, A. J. (2017). Microbial eukaryotes that lack sterols. *Journal of Eukaryotic Microbiology*, *64*, 897–900. https://doi.org/10.1111/jeu.12426

Taylor, S. R., & McLennan, S. M. (1985). *In the continental crust: Its composition and evolution*. Malden, MA: Blackwell Publishing.

Tribovillard, N., Algeo, T. J., Lyons, T. W., & Riboulleau, A. (2006). Trace metals as paleoredox and paleoproductivity proxies: An update. *Chemical Geology*, *232*, 12–32. https://doi.org/10.1016/j.chemgeo.2006.02.012

Volk, H., Dutkiewicz, A., George, S. C., & Ridley, J. (2003). Oil migration in the Middle Proterozoic Roper Superbasin, Australia: Evidence from oil inclusions and their geochemistries. *Journal of Geochemical Exploration*, *78*, 437–441. https://doi.org/10.1016/S0375-6742(03)00152-3

Volk, H., George, S. C., Dutkiewicz, A., & Ridley, J. (2005). Characterisation of fluid inclusion oil in a Mid-Proterozoic sandstone and dolerite (Roper Superbasin, Australia). *Chemical Geology*, *223*, 109–135. https://doi.org/10.1016/j.chemgeo.2004.12.024

Warren, J. K., George, S. C., Hamilton, P. J., & Tingate, P. (1998). Proterozoic source rocks: Sedimentology and organic characteristics of the Velkerri Formation, Northern Territory, Australia. *AAPG Bulletin*, *82*, 442–463.

Wei, J. H., Yin, X., & Welander, P. V. (2016). Sterol synthesis in diverse bacteria. *Frontiers in Microbiology*, *7*, 990.

Yang, S., Smith, T. M., Collins, A. S., Munson, T. J., Shoemaker, B., Nicholls, D., … Glorie, S. (2017). Uranium isotope compositions of mid-Proterozoic black shales: Evidence for an episode of increased ocean oxygenation at 1.36 Ga and evaluation of the effect of post-depositional hydrothermal fluid flow. *Precambrian Research*, *29*, 187–201. https://doi.org/10.1016/j.precamres.2017.06.016

Zumberge, J. A., Love, G. D., Cárdenas, P., Sperling, E. A., Gunasekera, S., Rohrssen, M., … Summons, R. E. (2018). Demosponge steroid biomarker 26-methylstigmastane provides evidence for Neoproterozoic animals. *Nature Ecology & Evolution*, *2*, 1709–1714. https://doi.org/10.1038/s41559-018-0676-2

SUPPORTING INFORMATION

Additional supporting information may be found online in the Supporting Information section at the end of the article.

How to cite this article: Nguyen K, Love GD, Zumberge JA, et al. Absence of biomarker evidence for early eukaryotic life from the Mesoproterozoic Roper Group: Searching across a marine redox gradient in mid-Proterozoic habitability. *Geobiology*. 2019;17:247–260. https://doi.org/10.1111/gbi.12329